Structure
Article

# Structure and Mechanism of the Lincosamide Antibiotic Adenylyltransferase LinB

Mariya Morar,[1] Kirandeep Bhullar,[1] Donald W. Hughes,[1] Murray Junop,[1] and Gerard D. Wright[1,*]
[1]M.G. DeGroote Institute for Infectious Disease Research, Department of Biochemistry and Biomedical Sciences and the Department of Chemistry, McMaster University, Hamilton, ON L8N 3Z5, Canada
*Correspondence: wrightge@mcmaster.ca
DOI 10.1016/j.str.2009.10.013

## SUMMARY

**Lincosamides make up an important class of antibiotics used against a wide range of pathogens, including methicillin-resistant *Staphylococcus aureus*. Predictably, lincosamide-resistant microorganisms have emerged with antibiotic modification as one of their major resistance strategies. Inactivating enzymes LinB/A catalyze adenylylation of the drug; however, little is known about their mechanistic and structural properties. We determined two X-ray structures of LinB: ternary substrate– and binary product–bound complexes. Structural and kinetic characterization of LinB, mutagenesis, solvent isotope effect, and product inhibition studies are consistent with a mechanism involving direct in-line nucleotidyl transfer. The characterization of LinB enabled its classification as a member of a nucleotidyltransferase superfamily, along with nucleotide polymerases and aminoglycoside nucleotidyltransferases, and this relationship offers further support for the LinB mechanism. The LinB structure provides an evolutionary link to ancient nucleotide polymerases and suggests that, like protein kinases and acetyltransferases, these are proto-resistance elements from which drug resistance can evolve.**

## INTRODUCTION

The lincosamide class of antibacterials originates from a natural product, lincomycin, and includes semisynthetic derivatives, clindamycin and pirlimycin (Figure 1). This class was first characterized in the 1960s and is now used for treatment of a broad spectrum of infections (Rezanka et al., 2007; Hoeksema et al., 1964). It is mostly active against gram-positive organisms, but also finds use against selected gram-negative anaerobes and protozoa. These antibiotics function by blocking microbial protein synthesis via binding to the 23S rRNA of the 50S subunit and mimicking the intermediate formed in the initial phase of the elongation cycle (Schlunzen et al., 2001; Fitzhugh, 1998). The most clinically relevant lincosamide, clindamycin, is frequently used to treat infections caused by streptococci and staphylococci. It is particularly useful in treatment of connective tissue infections because of its favorable skin and bone absorptivity and action against strains producing necrotizing toxins (Spizek et al., 2004). Clindamycin treatments have been limited in the past because of rapid development of resistance and gastrointestinal side effects.

Recently, as the emergence of multidrug-resistant pathogens has become a grave concern, lincosamide use has been revisited. In particular, clindamycin has been found to be potent in treating methicillin-resistant *Staphylococcus aureus* (MRSA), a pathogen causing worldwide concern because of its increasing rate of incidence and limited treatments (Bartlett, 2008; Johnson and Decker, 2008). Needless to say, increased antibiotic use leads to the development of resistance. Two of the most common routes of resistance to lincosamides include antibiotic modification, a route more prevalent in pathogenic gram-positive cocci (Dutta and Devriese, 1982; Leclercq et al., 1985), and methylation of the ribosomal 23S rRNA by Erm methyltransferases, observed in many genera and resulting in coresistance to macrolide and type B streptogramin antibiotics (Courvalin et al., 1985). Although the latter mechanism is now relatively well understood (Tu et al., 2005), the former has not been investigated in detail.

Organisms employing the antibiotic modification strategy inactivate lincosamides via adenylylation catalyzed by enzymes encoded by *lin* genes (Figure 2). Seven variations of the *lin* genes have been reported, and these have been divided into two groups on the basis of sequence analysis (Petinaki et al., 2008). One group includes LinA and its variants (LnuC and LnuD) and shows amino acid sequence homology with the aminoglycoside antibiotic nucleotidyltransferase ANT(2″)-Ia (Petinaki et al., 2008). LinA is found in staphylococci and is capable of adenylylation at either 3′- or 4′-OH of the methylthiolincosamide sugar of lincosamides (Brisson-Noel et al., 1988).

The second, smaller group, including LinB and LnuF, has sequence similarity with the β-subunit of the DNA polymerase (Pol β). LinB is found in enterococci, which are important pathogens in both human and veterinary medicine. These organisms are frequently the cause of nosocomial abdominal, pelvic, and postsurgical wound infections and are highly successful in acquisition of antibiotic resistance elements, resulting in the emergence of, among others, vancomycin-resistant enterococci (Sood et al., 2008). Understanding antibiotic resistance determinants from these organisms is therefore of great importance.

For LinB, clindamycin inactivation has been confirmed using Kirby-Bauer disk assay, and the inactivation product has been characterized by NMR (Bozdogan et al., 1999). The NMR analysis revealed that, unlike LinA, LinB modifies the 3′-OH of methylthiolincosamide only. In this work, we determined two X-ray crystal structures of *Enterococcus faecium* LinB. The ternary complex with the substrate, clindamycin, and nonhydrolyzable

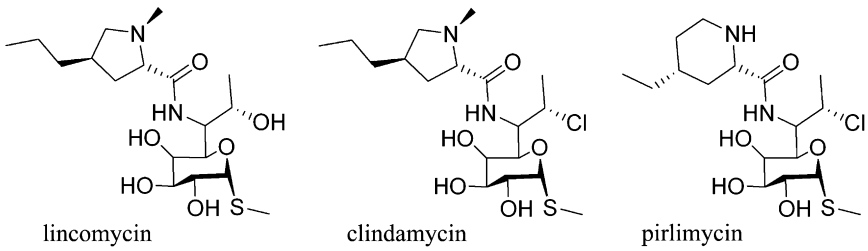


**Figure 1. Structures of the Common Lincosamide Class Antibiotics**
Figure was prepared using ChemDraw Ultra.

ATP analog, AMPCPP, enabled the identification of the active site and potential catalytic residues, which were subsequently examined by site-directed mutagenesis. The enzyme activity for the wild-type and mutated protein was quantified by determination of its steady-state kinetic parameters. The course of the reaction was further probed by solvent isotope effect and product inhibition experiments. On the basis of the structure-function studies, LinB was classified as a member of the nucleotidyltransferase (NT) superfamily, which includes aminoglycoside NTs and nucleotide polymerases. Collectively, biochemical and structural characterization and the comparison of LinB to structural and functional homologs allowed a proposal for the catalytic mechanism employed by this antibiotic resistance enzyme. Furthermore, analysis of the relationship of LinB to the NT superfamily members led to the classification of nucleotide polymerases as protoresistance genes in context of the evolution of drug resistance.

## RESULTS

### Overall Structure of LinB

The ternary and binary complex structures of LinB were refined to 2.0 Å and 2.1 Å resolution, respectively. The model of LinB contains 267 residues per monomer, all of which are present in the ternary complex. Residues 52–55, located in a small loop region, are missing as a result of disorder in the binary complex structure. The ligands for both complexes were modeled in manually, according to the corresponding Fo-Fc difference electron density maps. The final quality of the models was verified using PROCHECK (Laskowski et al., 1993), and the final R and $R_{free}$ values are listed in Table 1.

A protomer of LinB consists of two domains: an N-terminal and a C-terminal domain (Figure 3A). The N-terminal domain contains a six-stranded mixed β sheet flanked by two α helices on each side. The C-terminal domain is an α-helical bundle, which consists of five α helices. An extensive loop region connects the two domains.

The quaternary structure of LinB is most likely a dimer. LinB forms a dimer in the crystal by utilizing a noncrystallographic two-fold axis (Figure 3B). Analytical gel filtration chromatography data were consistent with a dimeric form of LinB in solution. The formation of a dimer is achieved by placement of the C-terminal bundle from one monomer in the cleft formed by the two domains of the second monomer. This swapped dimer arrangement results in formation of an extensive hydrogen-bonding network: C-terminal helix, α6, from one monomer interacts with the same helix of the second monomer, as does the loop connecting helices α7 and α8. Helices α5 and α9 of the bundle lie perpendicular to the strands β2, β3, β4, and β5 of the N-terminal domain of adjacent monomer. The loops involved in connecting the domains within the monomer are not part of the interface.

### LinB Active Site

Active site of LinB is located in a large cleft situated at the dimer interface (Figure 3B). In the ternary complex, clindamycin and a nonhydrolyzable nucleotide analog, AMPCPP, are present, as are two $Mg^{2+}$ ions chelated by both substrates (Figure 3C). The base and the ribose of the nucleotide are bound by the loop connecting the N- and C-terminal domain of one monomer, whereas the phosphate tail is sandwiched by the β sheet of the N-terminal domain of one monomer and C-terminal helices of the second monomer.

The base of AMPCPP forms no specific interactions with the enzyme and is largely exposed to solvent with N6 and N7 forming hydrogen bonds to water molecules. The 2′-OH of the ribose forms hydrogen bonds with water, whereas 3′-OH accepts a hydrogen bond from Lys32. Unlike the base and the sugar, the phosphate tail is locked in through an intricate network of interactions (Figure 3C). All three phosphates are chelated by one $Mg^{2+}$ ion (Mg1), and the α-phosphate is also chelated by the second $Mg^{2+}$ ion (Mg2). Two Ser residues from one monomer and two Arg residues from the second monomer form hydrogen bonds to β- and γ-phosphates of the analog. Both $Mg^{2+}$ ions are hexacoordinated. In addition to the three phosphates, Mg1 is coordinated by Asp40, Glu42, and a water molecule, whereas Mg2 is coordinated by Glu42, Glu89, Asp40,

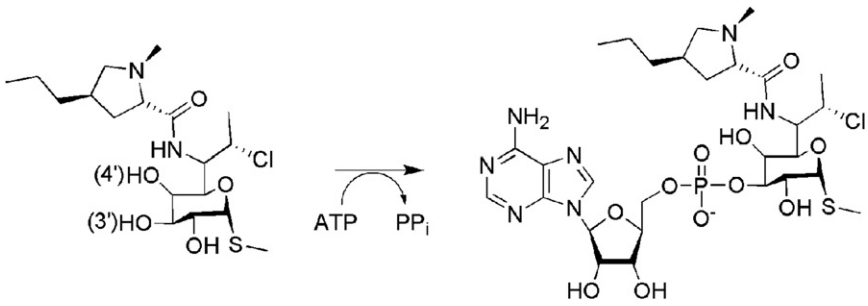


**Figure 2. Reaction Catalyzed by LinB**
Figure was prepared using ChemDraw Ultra. See also Tables S2–S4.

**Table 1. Data Collection and Refinement Statistics for LinB Structure Determination**

| Data Collection | LinB/PPi (SeMet) | LinB/AMPCPP/CLY |
|---|---|---|
| Resolution (Å) | 50–2.15 | 50–2.0 |
| Space group | $P2_12_12_1$ | $P2_12_12_1$ |
| Cell parameters | a = 63.99, b = 96.34, c = 103.65 | a = 63.69, b = 96.06, c = 102.71 |
| Unique reflections[a] | 67461 | 42525 |
| Redundancy | 6.4 (6.4)[b] | 3.3 (3.0) |
| Completeness (%) | 100 (100) | 98 (96) |
| I/σ | 19.8 (7.3) | 14.6 (3.8) |
| $R_{sym}$ | 9.4 (29.7) | 9.6 (36.8) |
| Data Refinement | | |
| R (%) | 17.9 | 16.8 |
| $R_{free}$ (%) | 22.2 | 22.1 |
| Reflections in work set | 34133 | 40327 |
| Reflections in test set | 1821 | 2130 |
| No of protein atoms | 4297 | 4407 |
| No of water | 450 | 751 |
| RMSD bond (Å) | 0.009 | 0.008 |
| Angle (°) | 1.1 | 1.1 |
| Mean B factor (Å$^2$) | 13.2 | 16.0 |

[a] Unique reflections include Bijvoet pairs.
[b] Values in parentheses are for the highest resolution shell.

3′-OH of clindamycin, α-phosphate of AMPCPP, and a water molecule. All residues involved in the binding of $Mg^{2+}$ ions come from the same monomer. Residues contributing to the phosphate tail and $Mg^{2+}$ ions binding are strictly conserved among LinB enzymes.

Clindamycin binding is confined to one monomer only, sandwiched between the AMPCPP molecule and the N-terminal β sheet. Unlike the base moiety of AMPCPP, the amino acyl moiety of clindamycin forms extensive hydrophobic interactions: partaking in these are Phe104, Tyr27, and Tyr44. This moiety forms T-stack interaction with the purine of AMPCPP. The peptide bond and the 4′-OH of the clindamycin sugar moiety form hydrogen bonds with Tyr44 and Tyr27, respectively. The 3′-OH interacts with Mg2 and Glu89, whereas 2′-OH interacts with the α-phosphate of AMPCPP.

The structure of the binary complex with pyrophosphate (PPi) reveals that the binding here is achieved via two Arg and two Ser residues and a $Mg^{2+}$ ion, exactly as seen for the β- and γ-phosphates of the AMPCPP phosphate tail.

### Kinetics Analysis and Mutagenesis

Turnover numbers and $K_M$ values for both substrates of LinB were determined in this work (Table 2). The high micromolar $K_M$ value for ATP and the low micromolar value for clindamycin are comparable with those for kanamycin nucleotidyltransferases, which are related to LinB structurally and functionally (Chen-Goodspeed et al., 1999). Enzyme inhibition was observed at higher concentrations of clindamycin, which could not be fitted to the standard substrate inhibition plot (data not shown). These observations are indicative of substrate interactions with LinB, which require further investigation.

On the basis of the structure, Glu89 was hypothesized to be important in the nucleotidyl transfer and Tyr27 in substrate binding and specificity. To further investigate the role of these residues in catalysis, Glu89 was mutated to alanine and glutamine, whereas Tyr27 was mutated to alanine. No enzymatic activity was observed for either E89A or E89Q mutant. LinB Y27A mutant showed a 10-fold reduction in the $k_{cat}$ value. Although the $K_M$ value for clindamycin was also reduced by 10 fold, that for ATP was essentially the same as that for the wild-type, indicating that Tyr27 is important for clindamycin binding.

### Solvent Isotope Effect

To investigate the possibility of 3′-OH deprotonation as a rate determining step in the reaction mechanism, the effects of substitution with 3′-OD were characterized. For this purpose, kinetic parameters of LinB were determined in $D_2O$ and compared with those in $H_2O$. Solvent isotope effects were minor for clindamycin with $k_{cat}^H/k_{cat}^D$ of 1.5 (Table 2). This result shows that, if indeed deprotonation is a catalytic step in the course of the reaction, this step is not rate determining.

### Effects of Product Inhibition

AMP-clindamycin is a competitive inhibitor of ATP, whereas no significant inhibition is observed for clindamycin (Figure 4). At high inhibitor concentrations, a plateau in ATP inhibition is observed, which is indicative of partial inhibition. LinB therefore follows an ordered mechanism, where ATP binding is the first step in the reaction and AMP-clindamycin release is the last.

## DISCUSSION

### Comparison of Substrate- and Product-Bound Structures

Comparison of the LinB ternary and binary complexes shows no significant conformational changes between the two structures. Minor movements of up to 1 Å are observed in the loop regions between strands β3 and β4 and between helices α3 and α4. The observed movements result in the active site cleft becoming slightly narrower upon clindamycin binding. The pyrophosphate is bound in the same position and at a nearly identical orientation as the β- and γ-phosphates of AMPCPP. The lack of structural changes between the two complexes, as well as similarity in binding of both the product and the substrate, indicates that the enzyme is unlikely to undergo major conformational changes during catalysis.

### Comparison with Other Nucleotidyltransferases (NTs)

On the basis of an iterative protein BLAST search (Altschul et al., 1990), *linB* analogs were found in seven organisms, with the protein sequence identity ranging from 80% to 100%. LinB shows sequence identity of 30% (50% similarity) with both *lnuF*, another lincosamide NT, and bacterial DNA polymeraseβ-subunit (Pol β). The alignment of the available sequences shows that all of the residues involved in the binding of the nucleotide are strictly conserved not only in LinB but also in LnuF and Pol β (Figure 5). On the other hand, the conservation of residues specific for clindamycin binding is mostly limited to LinB. This pattern in sequence conservation is consistent

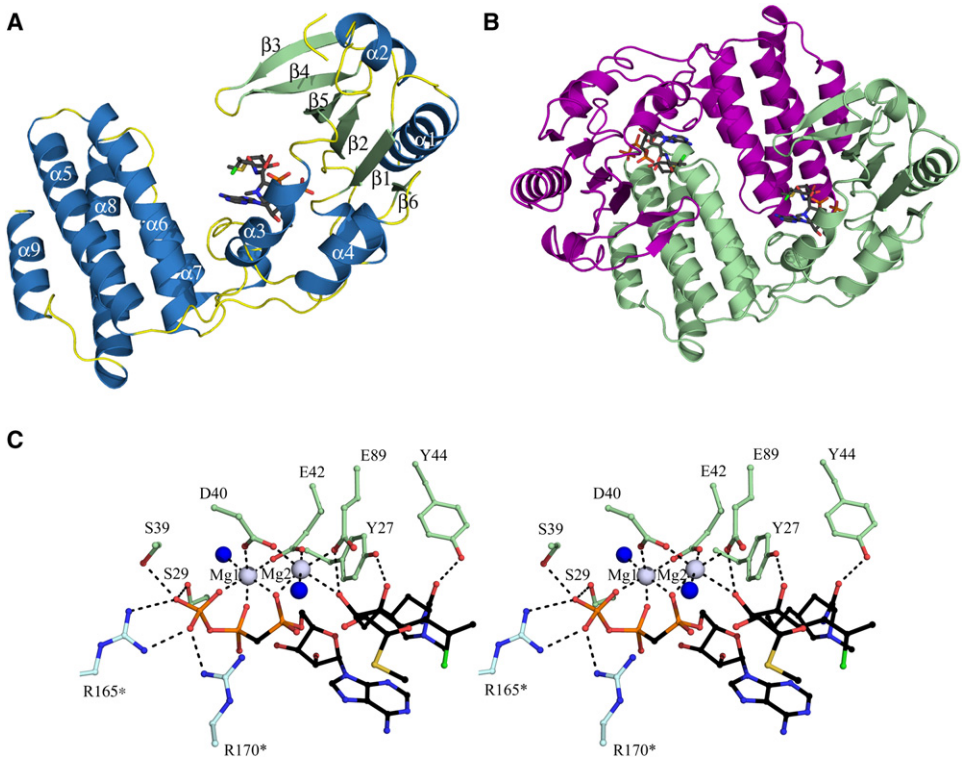


**Figure 3. Overall Structure of LinB**

(A) Ribbon diagram of the LinB monomer, color-coded by secondary structure. Helices are in blue, strands in green, and loops in yellow. Ligands, clindamycin, and AMPCPP are shown in ball-and-stick representation.

(B) Ribbon diagram of the LinB dimer: one monomer is shown in magenta, and the second monomer is in pale green. See also Figure S1.

(C) Stereo view of the LinB active site. Clindamycin and AMPCPP, ligands in the ternary complex of LinB, and residues forming interactions with the ligands are shown in ball-and-stick model. The ligands are color-coded, with C atoms in black, O atoms in red, N atoms in blue, S atoms in green, and P atoms in orange. The residues are color-coded same as the ligands, except C atoms are in pale green. $Mg^{2+}$ ions are shown as gray spheres, and water molecules as blue spheres. Hydrogen-bonding interactions are shown as dashed lines. Residue labels denoted by asterisk come from the adjacent monomer. The figure was prepared using Pymol and Photoshop.

with the ATP binding being the unifying feature for this group of NTs.

Dali analysis (Holm et al., 2008) was performed in search of structural homologs in the PDB (see Table S1 available online). This search revealed that LinB shares similarity with antibiotic NTs, of which *S. aureus* (Sa) KAN ANT(4′) is the only one biochemically characterized (Chen-Goodspeed et al., 1999; Pedersen et al., 1995). DNA polyA polymerase (PAP) structures were also detected (Martin et al., 2004; Meinke et al., 2008). Remarkably, all of these structures share less than 15% amino acid sequence identity.

**Table 2. Summary of LinB Kinetic Parameters at pH 7.5**

| | $k_{cat}$ ($s^{-1}$) | $K_M$ (μM) | $k_{cat}/K_M$ ($M^{-1}s^{-1}$) |
|---|---|---|---|
| Wild-type enzyme | | | |
| Clindamycin ($H_2O$) | $0.31 \pm 1 \times 10^{-4}$ | 3.7 ± 0.44 | $9 \times 10^4 \pm 227$ |
| Clindamycin ($D_2O$) | $0.15 \pm 7 \times 10^{-4}$ | 9.4 ± 2.0 | |
| MgATP | $0.6 \pm 5 \times 10^{-4}$ | 217 ± 23 | $2.8 \times 10^3 \pm 21$ |
| E89Q mutant | <0.003 | | |
| E89A mutant | <0.003 | | |
| Y27A mutant | | | |
| Clindamycin | $0.016 \pm 2 \times 10^{-4}$ | 73 ± 16 | 219 ± 13 |
| MgATP | $0.013 \pm 2 \times 10^{-4}$ | 441 ± 85 | 30 ± 2 |

Errors shown are standard errors to the fit of the data to Equation 1. See also Figure S2.

Of the four antibiotic NTs, two display similar quarternary organization, and all four share a similar fold and domain organization as LinB (Figure 6A). *Bacillus subtilis* (Bs) NT and SaANT(4′) are most similar with LinB, whereas the *Sulfolobus solfataricus* (Ss) NT lacks the C-terminal bundle and *Exiguobacterium sibiricum* (Es) NT has an additional domain after the C-terminal bundle, resulting in a greater dimer interface. On the basis of these comparisons, the N-terminal domain appears to be the minimal functional unit for the NT reaction with various structural accessories available for fine tuning.

Analysis of primary and secondary structure shows that the similarity extends to DNA polymerases PAP and Pol β, both of which also have structural elements of the β sheet sandwiched by α helices (Figure 6B). This similarity was initially observed with the first structures of KAN ANT(4′) (Sakon et al., 1993) and DNA Pol β (Davies et al., 1994; Sawaya et al., 1994), resulting in the identification of an ancient NT superfamily (Holm and Sander, 1995). The superfamily also includes terminal deoxyNT (TdT) (Delarue et al., 2002) and ATP:tRNA NT (CCAtr) (Okabe

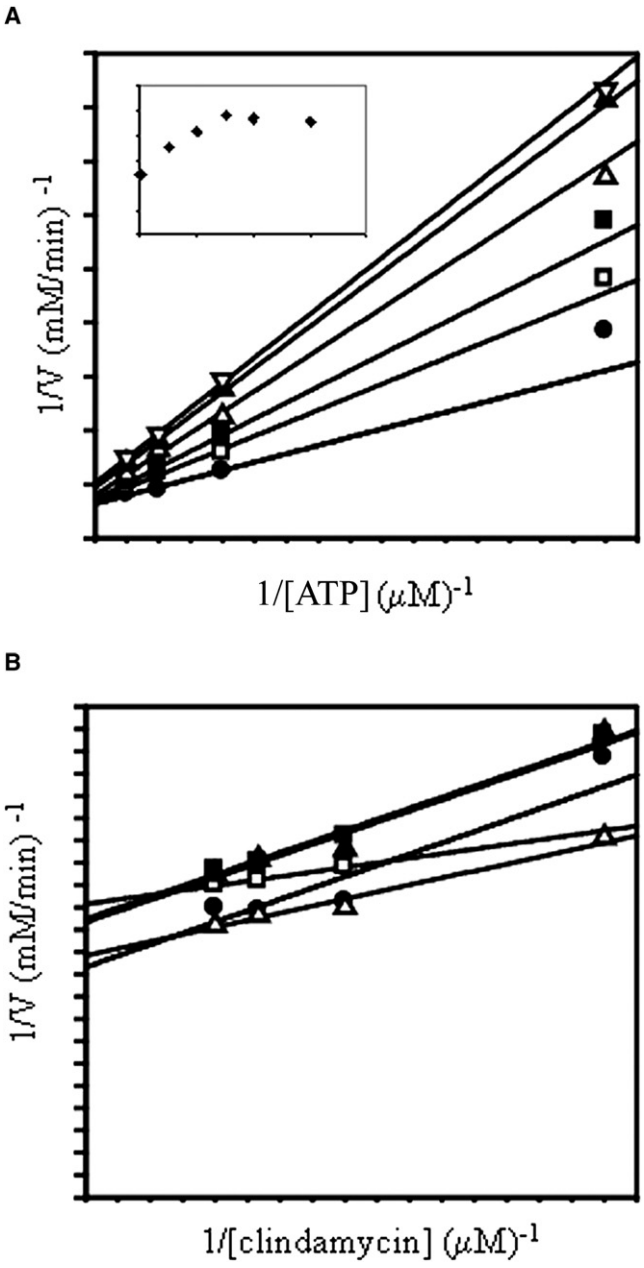


**Figure 4. Product Inhibition Effect**

(A) Double reciprocal plot of competitive inhibition of ATP by the purified product AMP-clindamycin. Concentrations of AMPclindamycin are 0 mM (●), 0.25 mM (□), 0.5 mM (■), 0.75 mM (△), 1 mM (▲), and 1.5 mM (▽). Inset is a replot of $K_{Mapp}$ versus KI.

(B) Lack of inhibition of clindamycin by AMP-clindamycin. Concentrations of AMP-clindamycin are 0.25 mM (●), 0.375 mM (□), 0.5 mM (■), 0.75 mM (△), and 0.9 mM (▲).

et al., 2003), whose structures have been determined. This structure of LinB expands this superfamily by adding lincosamide NTs to the growing collection.

Structural superposition reveals that not only is the fold conserved but also the three catalytic acidic residues responsible for the chelation of $Mg^{2+}$ ions (Figure 6C). For LinB, these are strictly conserved Asp40, Glu42, and Glu89, forming interactions with Mg1. The location of the $Mg^{2+}$ ion and the geometry with respect to the chelating residues is also maintained. Comparison of nucleotide binding shows that the adenine base and the ribose assume various conformations, whereas the geometry and interactions of the phosphate tail are conserved. Conservation of the catalytic residues and that of the $Mg^{2+}$ ion and the phosphate tail positioning all indicate a similar mechanism of action. As expected, residues responsible for the binding of clindamycin are not conserved because of great variation in the identity and the structure of second substrate within the superfamily.

## Mechanism of Action

In this work, the biochemical studies show that LinB readily inactivates clindamycin in vitro with the turnover of 0.3 $s^{-1}$, and the NMR analysis confirms the 3′-OH of clindamycin as the site of adenylylation. The map of the active site reveals the position of the two substrates, allowing for further discussion of the potential course of events. 3′-OH of clindamycin is bound by Glu89 and Mg1; the α-phosphate of AMPCPP also interacts with Mg1, which, in turn, is chelated by Glu89 (Figure 3C). The oxygen atom of the 3′-OH of clindamycin is 3.4 Å away from the phosphorus atom of the AMPCPP α-phosphate. The angle formed between the C3′, O3′, and Pα is 100°. The geometry of binding and distances between the reacting groups point to a direct in-line transfer of the adenylyl moiety onto clindamycin, making an adenylylated enzyme or other similar intermediates unlikely.

In-line AMP transfer mechanism is also supported by the body of literature discussing functional and structural relatives of LinB: ANTs and nucleotide polymerases. Ternary complex of SaANT(4′) with KAN and AMPCPP (Pedersen et al., 1995) and kinetic isotope effect studies (Gerratana et al., 2001) argue for direct in-line transfer for this enzyme. ANT(2″)-Ia is one of the earliest ANTs studied mechanistically and makes for an insightful comparison. For this enzyme, inversion of phosphorus configuration points to a simple direct nucleotidyl transfer (Van Pelt et al., 1986). Both ANT(4′) and ANT(2″)-Ia obey ordered mechanisms with the nucleotidylated product release being the last and the rate-limiting step (Chen-Goodspeed et al., 1999; Gates and Northrop, 1988). Our product inhibition experiments show that LinB also follows an ordered Bi-Bi mechanism.

Direct transfer could proceed via a dissociative mechanism with the formation of a metaphosphate-like transition state and pyrophosphate leaving prior to the attack onto clindamycin (Figure 7). The alternative is the activation of the 3′-OH for an in-line transfer to α-phosphate of ATP. This route is associative and would proceed via a pentacoordinated phosphate transition state (Figure 7). Both transition states have been described in the literature (Beard and Wilson, 2006; Thompson et al., 2002); however, in the case of LinB, the latter mechanism is more likely given the geometry of the active site.

Glu89 is proposed to be the catalytic base responsible for the activation of the 3′-OH. Mutagenesis of this residue confirmed that it is essential for catalysis. Glu89 forms a hydrogen bond with the reactive OH, and the abolishment of activity in a conservative mutation to a Gln residue is further indicative of

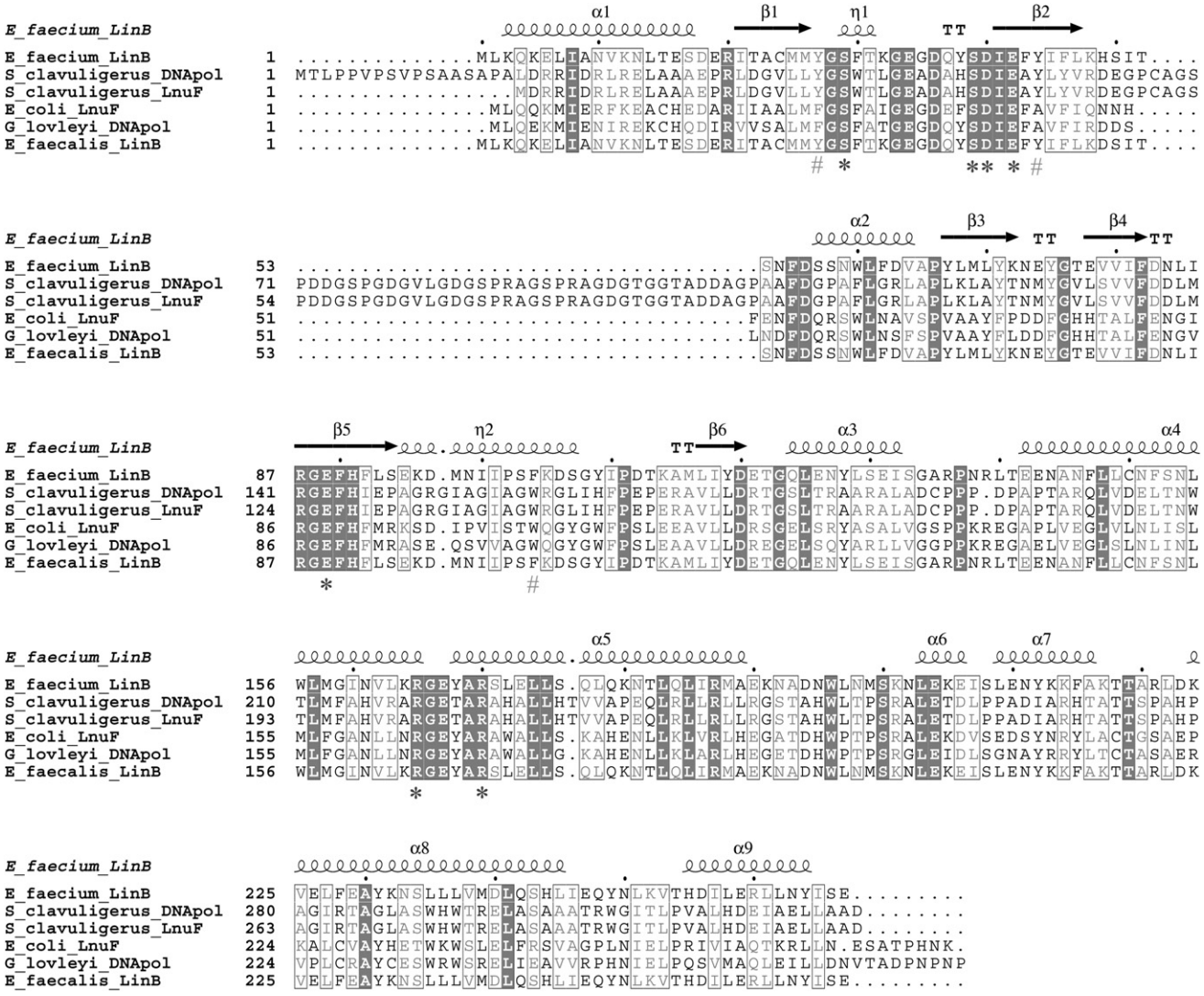


**Figure 5. Alignment of LinB, LnuF, and DNA Pol β Sequences Retrieved from BLAST Search**

Strictly conserved residues are highlighted gray, and conserved residues are in gray font. Secondary structural elements of LinB are shown at the top of the sequence. Asterisks at the bottom of the sequence indicate residues involved in the nucleotide binding; number signs indicate residues involved in clindamycin binding. The alignment was generated using ClustalW (Thompson et al., 1994) and rendered using ESPript (Gouet et al., 1999).

a function greater than binding and positioning of the substrate. An associative mechanism has been described for ANT(4′), the structural homolog of LinB, through the application of kinetic isotope effect experiments (Gerratana et al., 2001). Nucleotide polymerases overall, and specific members of the NT superfamily to which LinB belongs, also operate via such a mechanism, as illustrated by several crystal structures with trapped intermediate analogs (Steitz, 1998; Doublie et al., 1998; Sawaya et al., 1994; Batra et al., 2006). Although the mechanism with the substrate activation via a catalytic base is favored, the solvent isotope effect study shows that substrate deprotonation is not rate determining. Our observation is consistent with those for both ANT(4′) and ANT(2″)-Ia, where the product release is the slow step of the reaction (Chen-Goodspeed et al., 1999; Gates and Northrop, 1988).

## Implications of the LinB Structure and Mechanism in the Evolution of Antibiotic Resistance Genes

The relationship of the antibiotic modifying genes, lincosamide and aminoglycoside NTs, to nucleotide polymerases is now evident through this work and others. This relationship is likely the result of divergent evolution and is consistent with the hypothesis that the NTs responsible for antibiotic resistance arose from nucleotide polymerases. DNA and RNA polymerases are ancient and vital molecules found in all kingdoms of life. On the other hand, relatively few examples of lincosamide NTs are known, suggesting that these are the result of adaptation of certain organisms to their surrounding environment. The concept of the antibiotic resistome (Wright, 2007) states that resistance genes like *linB* that eventually make their way into pathogenic organisms originate in environmental organisms where

antibiotic producers, their neighbors, and related organisms have been using small molecules such as antibiotics to interact with each other for millennia. Bona fide resistance genes evolve from precursor genes by natural selection. Borrowing the vernacular of the oncogene field, we term these precursor genes "protoresistance" elements. Conservation of structure and mechanism between antibiotic resistance NTs and nucleotide polymerases described in this work indicates that, like protein kinases (Hon et al., 1997) and protein acetyltransferases (Wybenga-Groot et al., 1999), DNA polymerases are protoresistance elements implicated in the evolution of drug resistance. This information will facilitate future work to identify strategies, such as small molecule inhibitor discovery and design (Daigle et al., 1997), that can overcome antibiotic resistance.

## EXPERIMENTAL PROCEDURES

### Cloning, Expression, and Purification of LinB

The *linB* gene from *E. faecium* was synthesized with codon sequence optimized for expression in *Escherichia coli* and subcloned into pET28a expression vector (Novagen) by GenScript (USA). LinB containing plasmid was transformed into *E. coli* B834(DE3) expression cell line using a standard heat shock protocol. The resulting *E. coli* colonies were grown in 5 ml LB starter cultures supplemented with 40 μg/mL kanamycin (KAN) overnight at 37°C. The starter cultures were subsequently used to inoculate 1 L of LB culture with 40 μg/mL KAN. The 1 L culture was grown at 37°C until an $OD_{600nm}$ of 0.8 was reached and then was chilled in ice-water bath for 15 min. The protein expression was induced in the chilled culture with 100 μM IPTG, and the culture was further incubated overnight at 16°C. The cells were harvested via centrifugation using Avanti J25 centrifuge (Beckman) and were stored at −20°C until further use.

For protein purification, the cell pellet was resuspended in lysis buffer (100 mM HEPES [pH 7.5], 300 mM NaCl, and 10 mM imidazole). The cells were lysed via three passes through a French Pressure Cell (Aminco) at 13,000 psi, and the cell debris was removed via centrifugation at 30,000 *g*. The cleared supernatant was loaded onto a 5 ml Ni-NTA column (QIAGEN) and pre-equilibrated with lysis buffer at a flow rate of 1 mL/min. The column was then washed with a 100 ml volume of the lysis buffer, followed by step gradient wash with an elution buffer (100 mM HEPES [pH 7.5], 300 mM NaCl, and 250 mM imidazole). The gradient consisted of a 10% increase in the ratio of the elution buffer to the lysis buffer every 20 ml of wash. LinB eluted in 30–50% volume of the elution buffer. The enzyme purity was verified using SDS PAGE analysis, with the protein being approximately 90% pure. The protein solution was dialyzed overnight at 4°C into a dialysis buffer (10 mM Tris [pH 8.2] and 50 mM NaCl) and was concentrated to 50 mg/mL via Amicon-Ultra centrifugal device from Millipore. The protein concentration was determined using the Bradford Assay per the manufacturer's instructions (BioRad). The enzyme was then frozen and stored at −20°C until further use.

For structural studies, selenomethionine (SeMet) substituted protein was prepared. *E. coli* B834(DE3) cells transformed with LinB-containing pET28a plasmid were grown using the M9 SeMet high-yield growth media kit from Orion Biosolutions. The growth protocol provided by the manufacturer was followed. SeMet LinB was purified as described for the native enzyme, the only modification being the addition of 1 mM β-mercaptoethanol to all buffers.

### Analytical Gel Filtration

The oligomeric state of LinB in solution was determined via analytical gel filtration using a Superdex 200 10/300 GL column (GE Healthcare). The column was calibrated using a gel filtration LMW calibration kit (GE Healthcare) per the manufacturer's instructions. The elution buffer was 20 mM HEPES (pH 7.5) and 150 mM NaCl for all proteins. LinB eluted at 14.9 mL, corresponding to a molecular mass of 56 kDa. LinB elution profile and a table of elution volumes and molecular masses for proteins used are shown in Figure S1.

### Structure Determination

LinB was crystallized using a concentration of 13 mg/mL for native and 5 mg/mL for SeMet enzyme. The optimized crystallization conditions for LinB included 20% PEG3350, 0.1 M Tris (pH 8.5), and 0.1 M magnesium formate. Native LinB crystals were grown using hanging drop vapor diffusion method at 23°C. For the ternary complex, LinB was cocrystallized with 1 mM AMPCPP and 0.5 mM clindamycin (CLI). SeMet LinB was crystallized in the presence of 1 mM ATP. SeMet LinB crystal growth was induced by streak-seeding with native LinB crystals. LinB crystallized in the orthorhombic space group $P2_12_12_1$, a = 63.99 Å, b = 96.34 Å, c = 103.65 Å, 2 molecules per asymmetric unit, and 52% solvent content. The crystals were frozen in liquid nitrogen for data collection with the crystallization conditions supplemented with 17% glycerol used as cryoprotectant.

Single wavelength anomalous dispersion data were collected for the SeMet substituted crystals. The data were collected at the beamline X25C of National Synchrotron Light Source (Brookhaven, NY) using 0.9798 nm wavelength and 1° oscillation. HKL2000 program suite was used to index, integrate, and scale the data (Otwinowski and Minor, 1997). Data collection statistics are listed in Table 1. Ten Se sites of possible 16 were located and used for phasing using AutoSolve program in the Phenix program suite (Adams et al., 2002). The initial phases were used for electron density modification and automated model building in AutoBuild program in Phenix, resulting in the Cα-trace for 300 residues. The remaining backbone and side chains were then built manually using COOT software (Emsley and Cowtan, 2004). COOT was subsequently used in manual model refinement. Refmac5 program of CCP4 suite was used for rigid body and restrained refinement (Collaborative Computational Project, 1994; Potterton et al., 2003). Refinement statistics are listed in Table 1.

The data for the LinB/CLI/AMPCPP ternary complex were collected using RU300 rotating anode generator with the R-AXIS IV IP detector (MSC Ltd/Rigaku); 7 min exposure, 1° oscillation, and 200 mm crystal to detector distance. The HKL2000 program suite was used to index, integrate, and scale the data. The ternary complex structure was determined by molecular replacement using the dimer of the SeMet LinB structure as the search model and MolRep from CCP4 program suite to perform rotation and translation function calculations. COOT was used for manual refinement, and Refmac5 from CCP4 was used for automated refinement of the structure. Noncrystallographic symmetry restraints were used for the initial stages of the refinement. Data collection and refinement statistics are listed in Table 1.

### Kinetic Assays

The EnzCheck® pyrophosphate assay kit from Invitrogen, based on a previously described method, was used to quantify the kinetic parameters for the wild-type LinB (Upson et al., 1996). The kit was used as per Invitrogen protocol, and the reaction progress was monitored for 10 min at 360 nm. The modifications to the Invitrogen procedure follow. The 96-well flat bottom plates (Nalge NUNC Int.) were used in the experimental set-up, with the total volume of the reaction mixture being 250 μL. The reaction buffer was 50 mM HEPES (pH 7.5), 100 mM KCl, and 2 mM $MgCl_2$. The reaction was initiated using 10 μl of either clindamycin or ATP. When monitoring clindamycin dependence, 3 mM ATP was used, and final concentrations of clindamycin ranged between 3 and 300 μM. For ATP characterization, 50 μM clindamycin was used, and the ATP concentration ranged from 31 μM to 2 mM. For the calculations of the rate, a path length of 0.59 cm and an extinction coefficient of 11,000 $M^{-1}cm^{-1}$ were used. The initial rates were described by using Michaelis-Menten kinetics, as shown in Equation 1, with utility of Grafit 4 software (Erithacus Software, Staines, UK):

$$\nu = \frac{V_{max} \cdot [S]}{K_m + [S]}. \quad (1)$$

To assess the effects of site-directed mutagenesis (described below), Malachite-Green spectrophotometric assay was used. A previously described protocol for this assay was followed (De Leon et al., 2006). The activity of LinB-Y27A mutant was quantified using EnzCheck® pyrophosphate assay.

### Solvent Isotope Effect

Solvent isotope effects on the activity of LinB were assessed by quantifying the enzyme's kinetic parameters in 70% $D_2O$. EnzCheck® pyrophosphate assay was used with $D_2O$ used in place of $H_2O$ for the master mix dilutions.

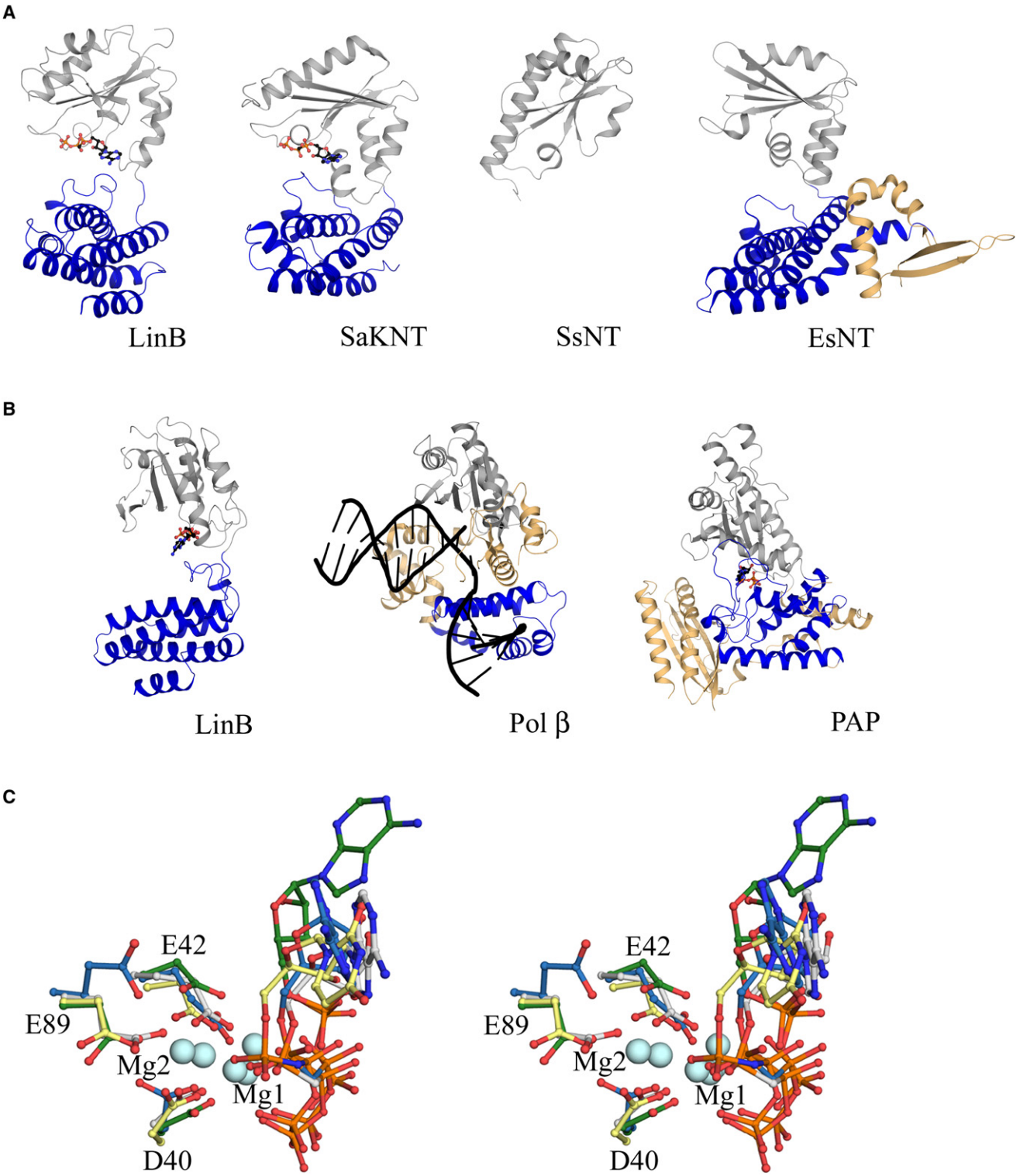


**Figure 6. Comparison of LinB Structure with the Members of the NT Superfamily**

(A) Structure of LinB is compared with aminoglycoside NT: SaANT(4′) (1kny), and putative antibiotic NTs: SsNT (2rff) and EsNT (3c18) illustrating the conservation of both the N and C-terminal domain. The N-terminal domains are in gray, C-terminal domains are in blue, and structural features missing from LinB are in light-orange.

(B) A ribbon diagram of the LinB structure compared with PAP and Pol β, illustrating the conservation of the N terminal domain. The N-terminal domain is in gray, α-helical bundle is in blue, and structural features missing from LinB are in light-orange.

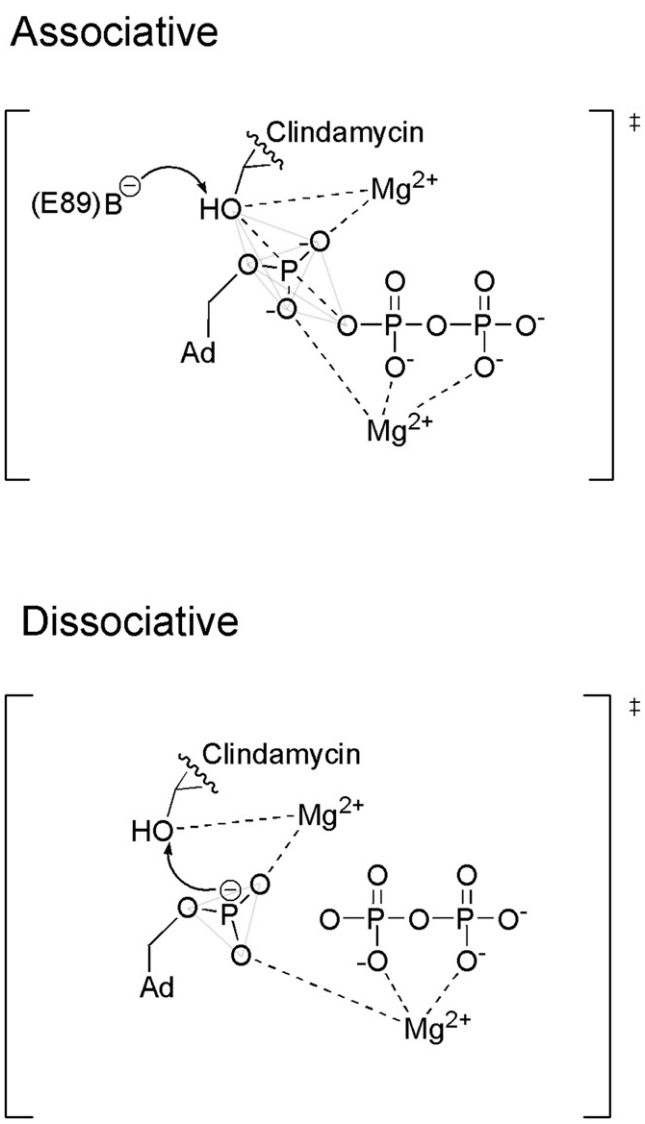


**Figure 7. Possible Transition States for the LinB Reaction**
Figure was prepared using ChemDraw Ultra.

### Enzymatic Synthesis of Adenylylated Clindamycin

For the product inhibition studies, adenylylated clindamycin (AMP-clindamycin) was synthesized and purified. Reaction mixture containing 100 μl of 50 mg/mL purified LinB, 20 mM HEPES (pH 7.5), 2 mM $MgCl_2$, and 3 mM ATP was initiated using 300 μl of 1.4 mg/mL clindamycin and incubated at room temperature for 1 hr. To purify the reaction product, high-pressure liquid chromatography was performed using DIONEX GP40 Gradient Pump. Aliquots of reaction mixture (100 μl) were injected onto C-18 reverse phase column (10 μm; 22 × 250 mm; GRACE VYDAC), and the pump flow rate was set to 1.0 mL/min. AMP-clindamycin was eluted using 70% Solvent A (0.03% trifluoroacetic acid in $H_2O$) and 30% Solvent B (0.03% trifluoroacetic acid in acetonitrile) in a linear gradient. Elution profile was monitored by a PDA-100 Photodiode Array Detector at 254 nm. Fractions were analyzed using QTrap LC/MS/MS System (Applied Biosystems/MDS SCIEX), and those of interest were pooled. Approximately 7 ml of purified product was collected and lyophilized overnight, yielding 14 mg of purified AMP-clindamycin. Powder sample was stored in −20°C and redissolved in appropriate buffers for further use. The structure of the purified product was confirmed by $^{1}H$ and $^{13}C$ NMR (Tables S2–S4).

### Product Inhibition Studies

The pyrophosphate assay was employed for product inhibition studies. Five different product concentrations were examined, and at each product concentration, that of one substrate was kept constant and that of the second substrate was varied. For the study of ATP inhibition, the concentrations of AMP-clindamycin were 0.25, 0.5, 0.75, 1, and 1.5 mM; those of ATP were 62.5, 250, 500, and 1000 μM; and that of clindamycin was 50 μM. For the study of clindamycin inhibition, the concentrations of AMP-clindamycin were 0.25, 0.375, 0.5, 0.75, and 0.9 mM; those of clindamycin were 6.25, 12.5, 18.75, and 25 μM; and that of ATP was 2 mM.

### Site-Directed Mutagenesis

QuikChange® Site-Directed Mutagenesis (Stratagene) was used to generate mutants of LinB in the pET28a vector as per manufacturer instructions. Primers used for mutagenesis are listed in Supplemental Experimental Procedures. The mutagenesis results were confirmed via DNA sequencing (MOBIX, McMaster University).

### Determination of Minimal Inhibitory Concentration (MIC)

MIC of clindamycin for the *E. coli* strains containing plasmids with wild-type and mutated LinB were determined by adapting the National Committee for Clinical Laboratory Standards protocol. The modification was the use of Luria-Bertani media for this experiment. Clindamycin has low activity against *E. coli*, and as expected the MIC for all strains was 128 μg/mL. Then, the bacterial growth was monitored every 30 min for 20 hr at 600 nm, showing impediment of growth during the exponential phase for strains containing LinB mutants E89Q and Y27A, as well as empty pET28a vector (Figure S2).

## ACCESSION NUMBERS

The coordinates and structure factors for the LinB/AMPCPP/CLI complex structure have been deposited to the Protein Data Bank under accession code 3JZ0, and that for LinB/PPi complex has been deposited under accession code 3JYY.

## SUPPLEMENTAL DATA

Supplemental Data include two figures and five tables and can be found with this article online at http://www.cell.com/structure/supplemental/S0969-2126(09)00420-1.

## ACKNOWLEDGMENTS

This work was supported by the Canadian Institutes of Health Research (grant MT-13536 to G.D.W.), the Canada Research Chairs program (support to G.D.W.), and Canadian Institutes of Health Research (grant MOP-89903 to M.J.).

Received: August 7, 2009
Revised: October 13, 2009
Accepted: October 14, 2009
Published: December 8, 2009

(C) Superposition of the active sites of LinB, SaANT(4′) (1kny), PAP (1q78), and Pol β (2fms). Nucleotides and the three acidic residues conserved within the superfamily are in ball-and-stick representation, and $Mg2^{+}$ ions are shown as spheres. The diagram is color-coded by atom type: C is gray for LinB, blue for SaANT(4′), green for PAP, and yellow for Pol β. Other atom types are colored the same as in Figure 1C. See also Table S1. The figure was prepared using Pymol and Photoshop.

## REFERENCES

Adams, P.D., Grosse-Kunstleve, R.W., Hung, L.W., Ioerger, T.R., McCoy, A.J., Moriarty, N.W., Read, R.J., Sacchettini, J.C., Sauter, N.K., and Terwilliger, T.C. (2002). PHENIX: building new software for automated crystallographic structure determination. Acta Crystallogr. D Biol. Crystallogr. *58*, 1948–1954.

Altschul, S.F., Gish, W., Miller, W., Myers, E.W., and Lipman, D.J. (1990). Basic local alignment search tool. J. Mol. Biol. *215*, 403–410.

Bartlett, J.G. (2008). Methicillin-resistant *Staphylococcus aureus* infections. Top. HIV Med. *16*, 151–155.

Batra, V.K., Beard, W.A., Shock, D.D., Krahn, J.M., Pedersen, L.C., and Wilson, S.H. (2006). Magnesium-induced assembly of a complete DNA polymerase catalytic complex. Structure *14*, 757–766.

Beard, W.A., and Wilson, S.H. (2006). Structure and mechanism of DNA polymerase Beta. Chem. Rev. *106*, 361–382.

Bozdogan, B., Berrezouga, L., Kuo, M.S., Yurek, D.A., Farley, K.A., Stockman, B.J., and Leclercq, R. (1999). A new resistance gene, linB, conferring resistance to lincosamides by nucleotidylation in *Enterococcus faecium* HM1025. Antimicrob. Agents Chemother. *43*, 925–929.

Brisson-Noel, A., Delrieu, P., Samain, D., and Courvalin, P. (1988). Inactivation of lincosaminide antibiotics in *Staphylococcus*. Identification of lincosaminide O-nucleotidyltransferases and comparison of the corresponding resistance genes. J. Biol. Chem. *263*, 15880–15887.

CCP4 (Collaborative Computational Project, Number 4). (1994). The CCP4 suite: programs for protein crystallography. Acta Crystallogr. D Biol. Crystallogr. *50*, 760–763.

Chen-Goodspeed, M., Vanhooke, J.L., Holden, H.M., and Raushel, F.M. (1999). Kinetic mechanism of kanamycin nucleotidyltransferase from *Staphylococcus aureus*. Bioorg. Chem. *27*, 395–408.

Courvalin, P., Ounissi, H., and Arthur, M. (1985). Multiplicity of macrolide-lincosamide-streptogramin antibiotic resistance determinants. J. Antimicrob. Chemother. *16* (Suppl A), 91–100.

Daigle, D.M., McKay, G.A., and Wright, G.D. (1997). Inhibition of aminoglycoside antibiotic resistance enzymes by protein kinase inhibitors. J. Biol. Chem. *272*, 24755–24758.

Davies, J.F., 2nd, Almassy, R.J., Hostomska, Z., Ferre, R.A., and Hostomsky, Z. (1994). 2.3 A crystal structure of the catalytic domain of DNA polymerase beta. Cell *76*, 1123–1133.

De Leon, G.P., Elowe, N.H., Koteva, K.P., Valvano, M.A., and Wright, G.D. (2006). An in vitro screen of bacterial lipopolysaccharide biosynthetic enzymes identifies an inhibitor of ADP-heptose biosynthesis. Chem. Biol. *13*, 437–441.

Delarue, M., Boule, J.B., Lescar, J., Expert-Bezancon, N., Jourdan, N., Sukumar, N., Rougeon, F., and Papanicolaou, C. (2002). Crystal structures of a template-independent DNA polymerase: murine terminal deoxynucleotidyltransferase. EMBO J. *21*, 427–439.

Doublie, S., Tabor, S., Long, A.M., Richardson, C.C., and Ellenberger, T. (1998). Crystal structure of a bacteriophage T7 DNA replication complex at 2.2 A resolution. Nature *391*, 251–258.

Dutta, G.N., and Devriese, L.A. (1982). Resistance to macrolide, lincosamide and streptogramin antibiotics and degradation of lincosamide antibiotics in streptococci from bovine mastitis. J. Antimicrob. Chemother. *10*, 403–408.

Emsley, P., and Cowtan, K. (2004). Coot: model-building tools for molecular graphics. Acta Crystallogr. D Biol. Crystallogr. *60*, 2126–2132.

Fitzhugh, A.L. (1998). Antibiotic inhibitors of the peptidyl transferase center. 1. Clindamycin as a composite analogue of the transfer RNA fragments L-Pro-Met and the D-ribosyl ring of adenosine. Bioorg. Med. Chem. Lett. *8*, 87–92.

Gates, C.A., and Northrop, D.B. (1988). Alternative substrate and inhibition kinetics of aminoglycoside nucleotidyltransferase 2″-I in support of a Theorell-Chance kinetic mechanism. Biochemistry *27*, 3826–3833.

Gerratana, B., Frey, P.A., and Cleland, W.W. (2001). Characterization of the transition-state structure of the reaction of kanamycin nucleotidyltransferase by heavy-atom kinetic isotope effects. Biochemistry *40*, 2972–2977.

Gouet, P., Courcelle, E., Stuart, D.I., and Metoz, F. (1999). ESPript: analysis of multiple sequence alignments in PostScript. Bioinformatics *15*, 305–308.

Hoeksema, H., Bannister, B., Birkenmeyer, R.D., Kagan, F., Magerlein, B.J., MacKellar, F.A., Schroeder, W., Slomp, G., and Herr, R.R. (1964). Chemical studies of lincomycin. 1. The structure of lincomycin. J. Am. Chem. Soc. *86*, 4223–4224.

Holm, L., and Sander, C. (1995). DNA polymerase beta belongs to an ancient nucleotidyltransferase superfamily. Trends Biochem. Sci. *20*, 345–347.

Holm, L., Kaariainen, S., Rosenstrom, P., and Schenkel, A. (2008). Searching protein structure databases with DaliLite v.3. Bioinformatics *24*, 2780–2781.

Hon, W.C., McKay, G.A., Thompson, P.R., Sweet, R.M., Yang, D.S., Wright, G.D., and Berghuis, A.M. (1997). Structure of an enzyme required for aminoglycoside antibiotic resistance reveals homology to eukaryotic protein kinases. Cell *89*, 887–895.

Johnson, M.D., and Decker, C.F. (2008). Antimicrobial agents in treatment of MRSA infections. Dis. Mon. *54*, 793–800.

Laskowski, R.A., MacArthur, M.W., Moss, D.S., and Thornton, J.M. (1993). PROCHECK: a program to check the stereochemical quality of protein structures. J. Appl. Cryst. *26*, 283–291.

Leclercq, R., Carlier, C., Duval, J., and Courvalin, P. (1985). Plasmid-mediated resistance to lincomycin by inactivation in *Staphylococcus haemolyticus*. Antimicrob. Agents Chemother. *28*, 421–424.

Martin, G., Moglich, A., Keller, W., and Doublie, S. (2004). Biochemical and structural insights into substrate binding and catalytic mechanism of mammalian poly(A) polymerase. J. Mol. Biol. *341*, 911–925.

Meinke, G., Ezeokonkwo, C., Balbo, P., Stafford, W., Moore, C., and Bohm, A. (2008). Structure of yeast poly(A) polymerase in complex with a peptide from Fip1, an intrinsically disordered protein. Biochemistry *47*, 6859–6869.

Okabe, M., Tomita, K., Ishitani, R., Ishii, R., Takeuchi, N., Arisaka, F., Nureki, O., and Yokoyama, S. (2003). Divergent evolutions of trinucleotide polymerization revealed by an archaeal CCA-adding enzyme structure. EMBO J. *22*, 5918–5927.

Otwinowski, Z., and Minor, W. (1997). Processing of X-ray diffraction data collected in oscillation mode. Methods Enzymol. *276*, 307–326.

Pedersen, L.C., Benning, M.M., and Holden, H.M. (1995). Structural investigation of the antibiotic and ATP-binding sites in kanamycin nucleotidyltransferase. Biochemistry *34*, 13305–13311.

Petinaki, E., Guerin-Faublee, V., Pichereau, V., Villers, C., Achard, A., Malbruny, B., and Leclercq, R. (2008). Lincomycin resistance gene lnu(D) in *Streptococcus uberis*. Antimicrob. Agents Chemother. *52*, 626–630.

Potterton, E., Briggs, P., Turkenburg, M., and Dodson, E. (2003). A graphical user interface to the CCP4 program suite. Acta Crystallogr. D Biol. Crystallogr. *59*, 1131–1137.

Rezanka, T., Spizek, J., and Sigler, K. (2007). Medicinal use of lincosamides and microbial resistance to them. Anti-Infect. Agents Med. Chem. *6*, 133–144.

Sakon, J., Liao, H.H., Kanikula, A.M., Benning, M.M., Rayment, I., and Holden, H.M. (1993). Molecular structure of kanamycin nucleotidyltransferase determined to 3.0-A resolution. Biochemistry *32*, 11977–11984.

Sawaya, M.R., Pelletier, H., Kumar, A., Wilson, S.H., and Kraut, J. (1994). Crystal structure of rat DNA polymerase beta: evidence for a common polymerase mechanism. Science *264*, 1930–1935.

Schlunzen, F., Zarivach, R., Harms, J., Bashan, A., Tocilj, A., Albrecht, R., Yonath, A., and Franceschi, F. (2001). Structural basis for the interaction of antibiotics with the peptidyl transferase centre in eubacteria. Nature *413*, 814–821.

Sood, S., Mahorta, M., Das, B.K., and Kapil, A. (2008). Enterococcal infections and antimicrobial resistance. Indian J. Med. Res. *128*, 111–121.

Spizek, J., Novotna, J., and Rezanka, T. (2004). Lincosamides: chemical structure, biosynthesis, mechanism of action, resistance, and applications. Adv. Appl. Microbiol. *56*, 121–154.

Steitz, T.A. (1998). A mechanism for all polymerases. Nature *391*, 231–232.

Thompson, J.D., Higgins, D.G., and Gibson, T.J. (1994). CLUSTAL W: improving the sensitivity of progressive multiple sequence alignment through sequence weighting, position-specific gap penalties and weight matrix choice. Nucleic Acids Res. *22*, 4673–4680.

 

Thompson, P.R., Boehr, D.D., Berghuis, A.M., and Wright, G.D. (2002). Mechanism of aminoglycoside antibiotic kinase APH(3′)-IIIa: role of the nucleotide positioning loop. Biochemistry *41*, 7001–7007.

Tu, D., Blaha, G., Moore, P.B., and Steitz, T.A. (2005). Structures of MLSBK antibiotics bound to mutated large ribosomal subunits provide a structural explanation for resistance. Cell *121*, 257–270.

Upson, R.H., Haugland, R.P., and Malekzadeh, M.N. (1996). A spectrophotometric method to measure enzymatic activity in reactions that generate inorganic pyrophosphate. Anal. Biochem. *243*, 41–45.

Van Pelt, J.E., Iyengar, R., and Frey, P.A. (1986). Gentamicin nucleotidyltransferase. Stereochemical inversion at phosphorus in enzymatic 2′-deoxyadenylyl transfer to tobramycin. J. Biol. Chem. *261*, 15995–15999.

Wright, G.D. (2007). The antibiotic resistome: the nexus of chemical and genetic diversity. Nat. Rev. Microbiol. *5*, 175–186.

Wybenga-Groot, L.E., Draker, K., Wright, G.D., and Berghuis, A.M. (1999). Crystal structure of an aminoglycoside 6′-N-acetyltransferase: defining the GCN5-related N-acetyltransferase superfamily fold. Structure *7*, 497–507.